Analysis and Interpretation of the Vibrational Spectrum of the Pyromellitic Dianhydride–Oxydianiline Polyimide and Its Charge-Transfer Complex with a Chromium Atom

B. D. Silverman

IBM Research Center, T. J. Watson Research Center, Yorktown Heights, New York 10598.
Received January 18, 1989; Revised Manuscript Received February 23, 1989

ABSTRACT: The vibrational levels of the pyromellitic dianhydride–oxydianiline (PMDA–ODA) polyimide have been calculated with the HONDO ab initio molecular orbital program. The calculated infrared active modes of significant intensity have been assigned to the previously observed peaks in the FT-IR spectrum of the polymer. The eigenvectors of these modes have been visually displayed and discussed in connection with a simulated HREELS spectrum. Changes in the mode frequencies and intensities upon formation of a half-sandwich complex composed of a single chromium atom with the PMDA ligand have also been investigated. Such changes are discussed in connection with changes in the observed HREELS experimental spectrum one might expect during the initial stages of formation of the chromium–PMDA–ODA polyimide interface.

I. Introduction

High-resolution electron energy loss spectroscopy (HREELS) has recently been utilized[1-5] in the characterization of the pyromellitic dianhydride–oxydianiline (PMDA–ODA) polyimide surface as well as in the characterization of interfaces created from vapor deposition of chromium and aluminum onto the PMDA–ODA surface. Information obtained from these measurements supplements information obtained from the more extensively utilized X-ray photoemission (XPS) and ultraviolet photoemission (UPS) spectroscopic techniques.[6-9] In connection with these latter spectroscopic techniques, we have previously performed molecular orbital calculations,[10-13] in an attempt to assist in understanding the chemistry of the PMDA–ODA polymer surface, as well as what occurs during the initial stages of chromium deposition onto such a surface. Since the HREELS results are so striking, we thought that it would be of interest to extend our previous calculations to include consideration of the molecular vibrations of the polymer. Hopefully, such calculations should assist in the interpretation of the infrared spectral data[14] and the HREELS data[1-5] obtained on the polymer.

II. Methods

Figure 1a shows the repeat unit of the pyromellitic dianhydride–oxydianiline polyimide. Since many or most of the vibrational degrees of freedom probed by the HREELS measurements involve internal degrees of freedom of this structural unit, attention has been focused on just this molecular unit. Furthermore, since a molecular complex involving both the PMDA and ODA segments is too large for us to treat by the HONDO ab initio molecular orbital program, the segments have been treated separately. This is consistent with our previous strategy in determining the photoemission characteristics of the polymer. Figure 1b shows the pyromellitic–diimide fragment, and Figure 1c shows the oxydianiline fragment that will be examined. Superposition of the results obtained for these two molecules should, however, yield an approximate representative characterization of the PMDA–ODA repeat unit (Figure 1a). The calculations are performed as follows: First, one performs a geometry optimization of each of the fragments using the HONDO ab initio molecular orbital program.[15] Then, with this optimized geometry as input to the HONDO program, the vibrational analysis is performed. We have utilized the 3-21g basis[16] in all of the calculations. Apparently, this represents a good and economical basis to use in calculations performed on such relatively large molecular fragments. Calculations have also been performed on the one-to-one chromium–PMDA half-sandwich complex that we had previously investigated in connection with the analysis of photoemission spectra obtained on the chromium–polyimide interface. Even though this complex is unsaturated, we believe that the computational results for the complex mimic features obtained when single chromium atoms, during the initial stages of vapor deposition, interact in the vicinity of the polymeric surface. Calculations that we have performed on saturated, tightly bound chromium–PMDA dimer complexes, with structures consistent with expected local ordering,[17] have been found to yield results that qualitatively parallel the electronic properties found for the simpler unsaturated one-to-one half-sandwich complex. For the present vibrational computations, the chromium atom basis utilized is the Dobbs–Hehre 3-21g split-valence basis.[18] All calculations performed are at the restricted Hartree–Fock self-consistent-field (RHFSCF) level of approximation.

Table I
Optimized Bond Lengths of the PMDA Fragment

bond	length, Å	for Cr complex, Å
C1–C6	1.38	1.39
C5–C7	1.38	1.51
C5–C9	1.50	1.45
C9–N17	1.39	1.40
C9–O13	1.202	1.213

Table II
Optimized Bond Lengths of the ODA Fragment

bond	length, Å	bond	length, Å
O1–C2	1.39	C16–C18	1.38
C2–C4	1.38	C6–C8	1.39
C2–C18	1.38	C8–C16	1.39
C4–C6	1.38	C8–N10	1.38

III. Optimized Geometries

A. PMDA and ODA Optimized Geometries. Tables I and II list the bond lengths obtained for the PMDA and ODA molecular fragments. The atomic designations are given in Figures 2 and 3. The fragments have been constrained to have D_{2h} and C_2 symmetry, respectively. The carbonyl bond length of 1.202 Å is comparable with the value of 1.207 Å, obtained previously[16] for this bond in formaldehyde. All of the carbon–carbon bond lengths of the central benzene ring are approximately 1.38 Å, i.e., near the expected aromatic value of 1.39 Å. For the ODA molecular fragment (Figure 3), we have found the torsion angle, C2–O1–C3–C19, to be 39.8 deg. The angle between

0024-9297/89/2222-3768$01.50/0

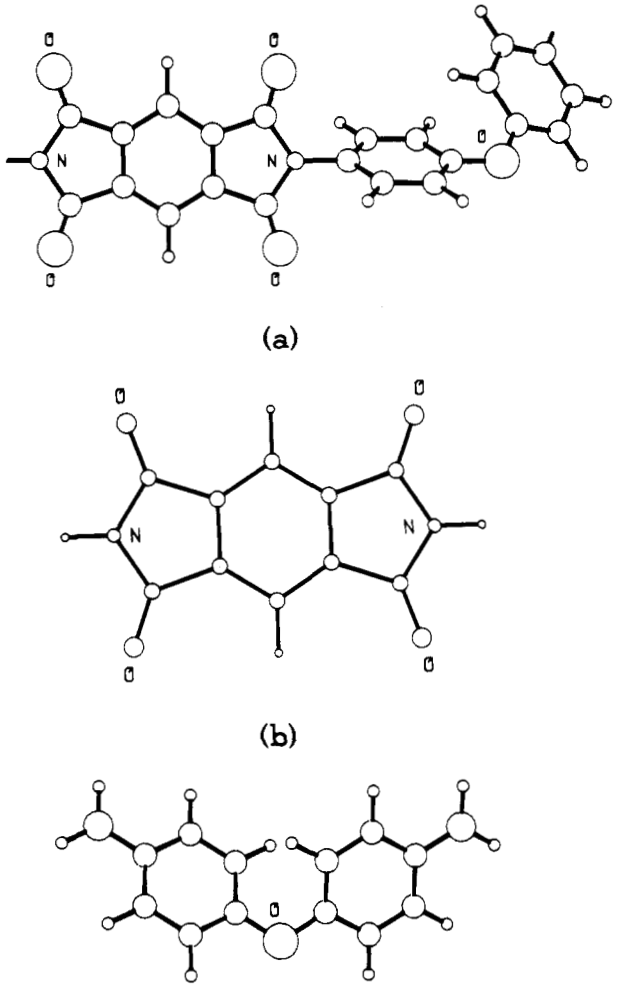

Figure 1. Structural units of the PMDA–ODA polyimide. (a) Repeat unit of the polymer. (b) PMDA fragment. (c) ODA fragment.

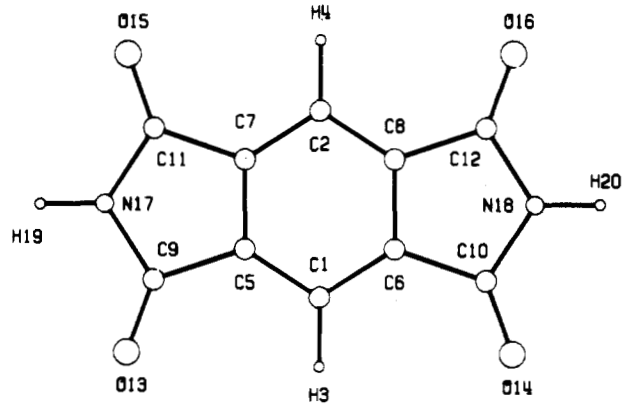

Figure 2. Atomic numbering of the PMDA unit.

the planes of the two phenyl groups is 70 deg. The C–O–C bond angle is 123 deg.

B. Chromium–PMDA Complex Optimized Geometry. In the formation of the unsaturated coordination complex between a chromium atom and the PMDA unit, one orbital that plays a crucial role in the bonding is the lowest unoccupied PMDA molecular orbital (LUMO). Two three-dimensional views of this orbital are illustrated[19] in Figure 4. This is the orbital involved in the so-called "back-charge donation" from chromium to the ligand. The amplitude of this orbital is seen to be distributed primarily

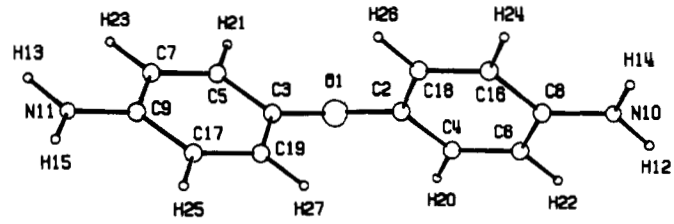

Figure 3. Atomic numbering of the ODA unit.

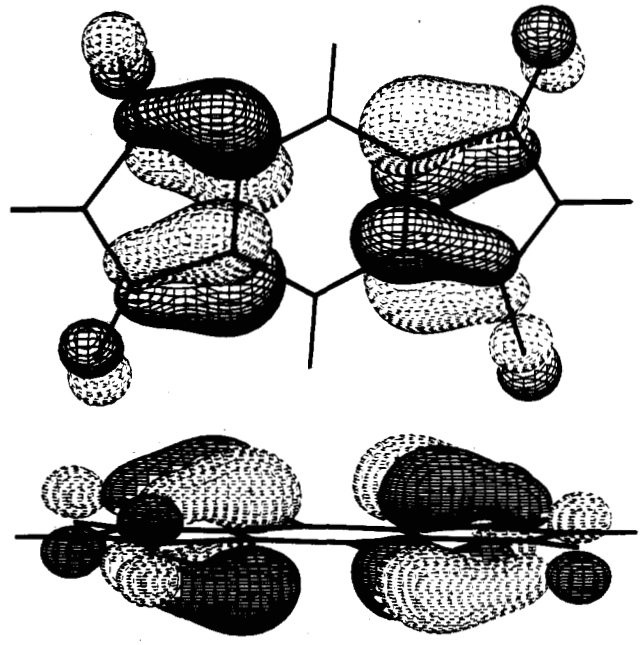

Figure 4. Two views of the PMDA lowest unoccupied molecular orbital (LUMO).

Table III
Mulliken Electronic Charge of Atoms of the PMDA Fragment

atom	charge	for Cr complex
C1	6.096	5.951
C5	6.172	6.557
C9	5.046	5.069
O13	8.576	8.625
N17	7.974	7.971

at the four carbon atoms of the central benzene ring. There is also amplitude at the four carbonyl oxygen atoms, with lesser amplitude on the carbonyl carbon atoms. The details of the quantum chemistry associated with the formation of this complex have been previously discussed.[13] Table III lists the Mulliken electronic charge[15] at each of the atomic centers of the PMDA fragment before and after complexing with chromium. One sees that the charge transferred from chromium to the ligand is distributed in a manner consistent with the distribution of LUMO amplitudes at the atoms composing PMDA. Figure 5 shows two three-dimensional views of the wave function amplitude of the highest occupied molecular orbital (HOMO) of the chromium–PMDA complex. The phase of the d_{xy} chromium orbital is just appropriately matched to the phase of the ligand LUMO (Figure 4) so that the orbital amplitudes just appear to continuously merge in Figure 5. Such phase matching contributes significantly to the bonding of this complex. In Figures 4 and 5, the same single contour value has been used in generating the three-dimensional plots. In Figure 5, the bonds between the chromium atom and the carbon atoms C1 and C2 (Figure 2) are not connected since these bond lengths are just above the cutoff value of the program. The bond

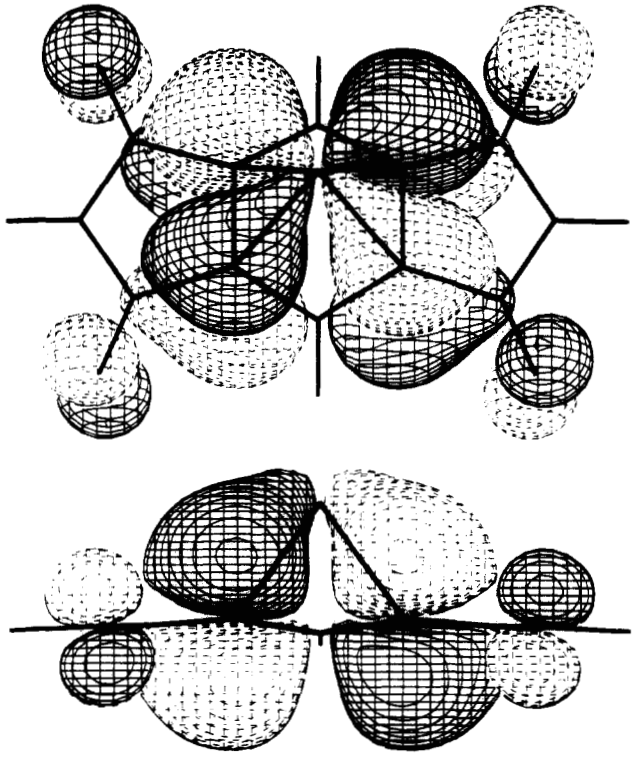

Figure 5. Two views of the Cr–PMDA highest occupied molecular orbital (HOMO).

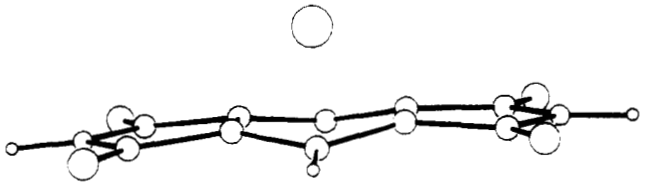

Figure 6. Optimized 3-21g structure of the chromium–PMDA complex.

lengths between the chromium atom and C5, C6, C7, and C8 are shorter.

Table I lists the covalent bond lengths found for the geometry of the optimized complex along with the values obtained prior to complexing. One notes the significant increase in length of the C5–C7 bond. It increases from a characteristic aromatic bond length to a value more closely identified with C–C single bond character. Such a change in bond character is also presumably driven by the large increase in electronic charge at these two atomic centers upon complexing with chromium. One should also note the significant but lesser elongation of the carbonyl bond length upon complex formation. From these changes, one can infer that vibrational modes involving significant relative motion of C5 with respect to C7 (similarly C6 with respect to C8) will exhibit a reduction in frequency upon complex formation. This is indeed what we have found in the vibrational analysis. Such frequency lowering should also be found for the carbonyl modes. Since the symmetry is reduced from D_{2h} to C_{2v} upon complexing with chromium, one expects that the PMDA molecule will, in general, no longer be planar. Figure 6 shows the buckled complex obtained with the 3-21g geometry optimization. This buckling is also seen in the edge-on view of Figure 5.

IV. Vibrational Spectrum

A. Vibrations of the Clean Polyimide. Figure 7 shows the calculated IR spectrum obtained by superposing the calculated vibrational spectra for the PMDA and ODA

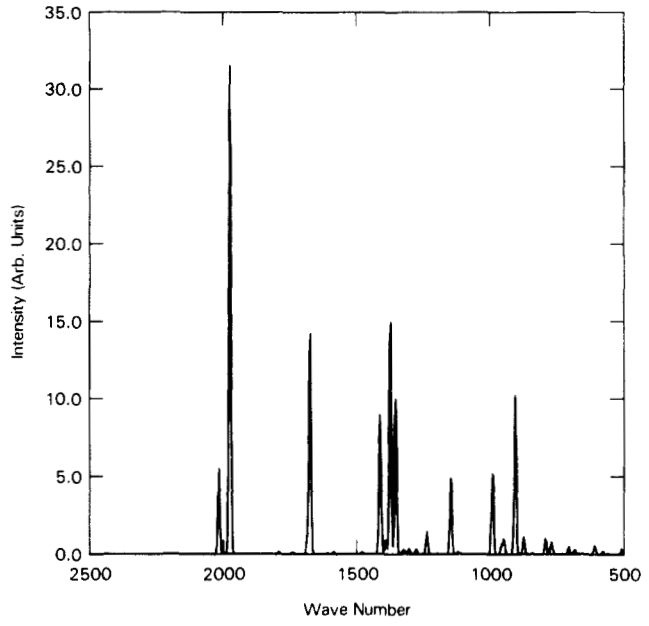

Figure 7. Calculated IR spectrum.

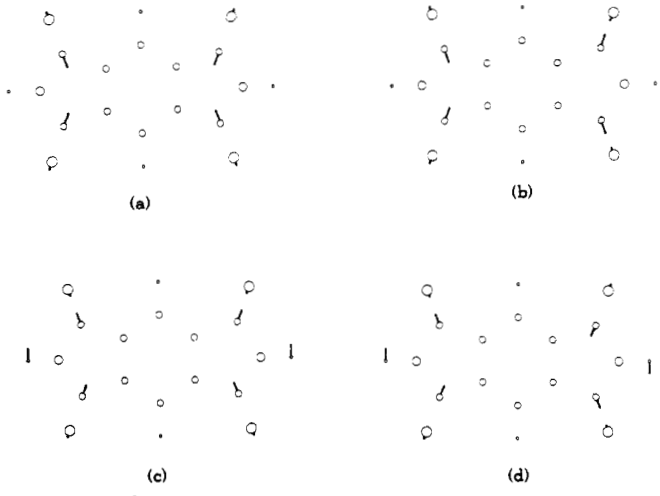

Figure 8. Carbonyl eigenmodes of PMDA. (a) Eigenmode of A_g symmetry at 1791 (2032) cm^{-1}. (b) Eigenmode of B_{3u} symmetry at 1779 (2018) cm^{-1}. (c) Eigenmode of B_{2u} symmetry at 1742 (1976) cm^{-1}. (d) Eigenmode of B_{1g} symmetry at 1739 (1973) cm^{-1}.

molecular fragments. This spectrum has been calculated by assuming isotropy, i.e., by averaging equally over all polarization directions. To generate the figure, each mode has been Gaussian broadened by 5 cm^{-1}. We have also deleted the modes composed of essentially only vibrations of the hydrogen atoms used to terminate the molecular fragments of the polymer. This figure should be compared with Figure 7 of ref 13. First, one notes that the most prominent feature over the IR spectral range is the high-frequency feature reflecting the carbonyl vibrations. Furthermore, looking at the abscissa, one notes that the calculated curves are shifted up in frequency from the experimental values by approximately 10%. This overestimate of vibrational frequencies obtained with the 3-21g basis is apparently a general feature of such calculations.[16,20] A more accurate determination of molecular vibrational frequencies has been achieved for smaller molecules, e.g., acetylene, with use of a larger set of basis functions, inclusion of electron correlation as well as effects of anharmonicity.[21]

Figure 8 illustrates the eigenmodes associated with the carbonyl vibrations of the PMDA unit. There are four such modes for the centrosymmetric PMDA unit that we

Table IV
Calculated Infrared Active Frequencies (cm^{-1}) (with Inclusion of All of the Carbonyl Vibrations)

			for Cr complex	
PMDA	$A_g(8)^a$	1791 (2032)	A_1	1733 (1966)
PMDA	$B_{3u}(8)$	1779 (2018)	B_1	1708 (1937)
PMDA	$B_{2u}(8)$	1742 (1976)	B_2	1699 (1927)
PMDA	$B_{1g}(8)$	1739 (1973)	A_2	1691 (1918)
ODA	B(10)	1477 (1675)		
PMDA	$B_{3u}(19)$		$B_1(19)$	1415 (1605)
PMDA	$B_{3u}(11)$	1247 (1414)	$B_1(20)$	1242 (1409)
ODA	B(12)	1212 (1375)		
PMDA	$B_{3u}(13)$	1195 (1355)	$B_1(21)$	1226 (1391)
PMDA	$B_{2u}(14)$	1011 (1147)	$B_2(22)$	1017 (1154)
ODA	A(15)	876 (994)		
ODA	B(16)	873 (990)		
PMDA	$B_{1u}(17)$	799 (906)	A(23)	840 (953)

[a] The mode displacements are illustrated in the figure whose number is given in parentheses just after the symmetry mode type.

have examined. The high-frequency infrared inactive "breathing" mode of A_g symmetry, Figure 8a, is found at 2032 cm^{-1}, respectively. The next two infrared active modes, exhibiting B_{3u} (Fig. 8(b)) and B_{2u} (Figure 8c) symmetry, are found at 2018 and 1976 cm^{-1}, respectively. The B_{3u} mode is the so-called "in-phase mode", with carbonyl vibration of each of the imide functionalities, in-phase. The B_{2u} mode, the so-called "out-of-phase" mode, has out-of-phase carbonyl vibrations on each of the imide rings. From the eigenvector diagram, one sees simply that B_{2u} transforms as y, i.e., along the direction perpendicular the the long axis of the molecule, whereas B_{3u} transforms as x, along this long axis. The calculated ratio of the infrared intensities of mode B_{2u} with respect to mode B_{3u} is 6.0. This relatively large value is essentially a reflection of the orientation of the dipole generated by the carbonyl atomic displacements. This dipole moment is aligned more closely along the short axis of the molecule. The lowest frequency carbonyl mode calculated to be at 1973 cm^{-1} is the Raman active mode of B_{1g} symmetry. Experimentally, the infrared active in-phase carbonyl mode has been found at 1779 cm^{-1}, whereas the out-of-phase mode has been found[14] at 1725 cm^{-1}. To enable a simpler qualitative comparison between all calculated vibrational frequencies and the experimentally observed values, we will scale all calculated vibrational frequencies so that the in-phase vibrational component is exactly equal to the experimental value. We therefore reduce all of the vibrational frequencies to 88.16% of their calculated values. This scaled value will be given throughout the text of the paper as well as in Table IV. The unscaled calculated value will be given in parentheses, just after this scaled value throughout the text. Table IV lists all calculated frequencies with significant calculated infrared intensity as well as all of the carbonyl frequencies.

Figure 9 simulates the HREELS data using the calculated spectrum. To obtain this figure, we have Gaussian broadened each of the vibrational levels by 85 cm^{-1} and plotted the spectrum over a wider range of frequency than for the calculated IR spectrum and in the reverse order from that given in Figure 7. As for the calculated IR spectrum (Figure 7), we have assumed an isotropic average over the infrared active modes. This figure should be compared with Figure 2 of ref 5. We have also shifted the abscissa so that the calculated frequencies are scaled down in magnitude as previously described. The relationship between FT-IR and HREELS intensities is not straightforward; however, it has been pointed out[5] that a relatively close correspondence can be made between the vibrational frequencies obtained by the two different techniques. As

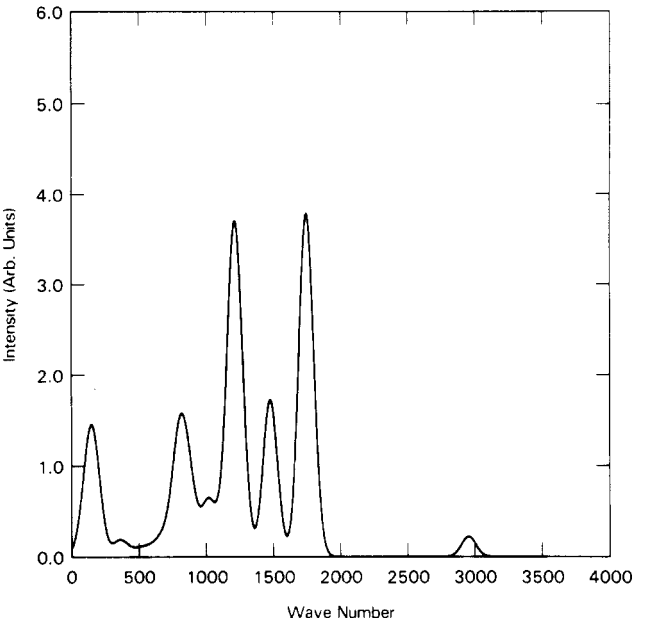

Figure 9. Simulated HREELS spectrum from the calculated infrared active vibrational frequencies.

a first approximation, we have therefore used the calculated IR intensity as a measure of intensity of the HREELS spectrum. One expects that this will yield results that at least parallel the HREELS spectrum obtained in the specular reflection regime.[22,23] Comparing Figure 9 with the experimental HREELS data,[5] one first notices the significantly larger HREELS intensities associated with the C–H stretching frequencies. It is well-known that such stretching modes are less intense in the FT-IR than as observed in HREELS.[2]

Below 2000 cm^{-1}, it is of interest that, even though the detailed shapes of the observed and calculated HREELS spectrum are different, there is a correspondence between the regions exhibiting enhanced spectral density. As previously mentioned, Table IV lists the modes of calculated enhanced infrared intensity as well as all of the carbonyl modes.

The first intense band of the calculated spectrum is centered near 1750 cm^{-1} and arises from the two infrared active carbonyl vibrations. Most of the contribution to this peak is from the out-of-phase vibration since this is the vibration with large dipole moment along the short axis of the molecule, i.e., the direction most nearly aligned with the carbonyl direction. The in-phase weaker component is apparently not observed in the HREELS measurements.[5] This calculated relative intensity of the two carbonyl spectral components is consistent with the observed FT-IR intensities.[14]

The next calculated HREELS peak arises from the ODA molecule and is centered at 1477 (1675) cm^{-1}. The eigenvector of this mode of B symmetry is shown in Figure 10. Two views are given. They are related by a 180-deg rotation about an axis through the long direction of the ODA fragment. This mode can be identified as the mode of strong observed[14] intensity in the FT-IR at 1505 cm^{-1}. A word about how Figure 10 has been generated is necessary. Some thought was given concerning how to display the eigenvector information visually. In general, one has a molecular structure that is three dimensional (such as in the case of the ODA molecule) and a set of three-dimensional displacements associated with each atom of the molecule. We wanted to generate a three-dimensional view of the displacements with perspective. We also wanted the ability to rotate the structure and the atomic dis-

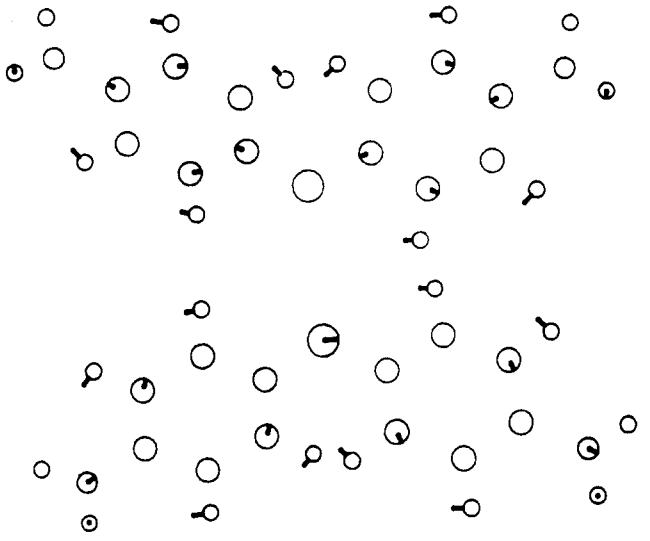

Figure 10. Eigenvector of the B mode of ODA at 1477 (1675) cm^{-1}.

placements by an arbitrary angle about any axis in three dimensions. This was achieved simply by modifying the input to the ORTEP-II molecular structure graphics program.[24] Two sets of atomic positions were generated; the atomic coordinates at the equilibrium positions and the atomic coordinates of the atoms at the positions of normalized amplitude for the vibration associated with a particular mode. The atoms at the equilibrium positions were drawn as spheres with radii reflecting their atomic type. These atoms were then joined to the positions at normalized amplitude by lines. Bonds connecting the atoms at their equilibrium positions were not drawn as is usually done. Since this program utilizes hidden line erasure, some care must be taken in viewing the displacements associated with the eigenvector. For the present work, this is true only for the ODA eigenmodes. For example, in Figure 10 which shows two views of the eigenvector of the ODA mode located at 1477 (1675) cm^{-1}, one of the views shows motion of the ether oxygen atom whereas the other view does not. The small line segment describing the motion in one of the views is behind the ether oxygen atoms as drawn and therefore does not appear since it is a hidden line. This is the reason that two different views of the eigenvectors of the ODA vibrational modes are shown. The two views of the ODA molecule shown in Figure 10 are related by a 180-deg rotation about the long axis of the molecule. All pairs of ODA eigenvectors that we will illustrate are so related. The eigenvectors of the chromium–PMDA complex will be illustrated with a view perpendicular to the plane of the ligand prior to its complexing and subsequent buckling. Mode displacements normal to this plane are negligible for the chromium–PMDA vibrational eigenvectors that will be displayed.

The next peak in the calculated HREELS spectrum (Figure 9) is actually a superposition of three vibrations. The highest mode frequency is at 1247 (1414) cm^{-1}. It is a B_{3u} mode of the PMDA unit. The eigenvector of this mode is shown in Figure 11. It involves significant deformation of the imide ring of the molecule. One might identify this mode with the mode observed at 1383 cm^{-1} in the FT-IR.[14] The next mode is calculated to be at 1212 (1375) cm^{-1}. Two views of the eigenvector of this ODA vibrational mode of B symmetry are shown in Figure 12. It is interersting to note that both this mode as well as the higher lying infrared active ODA mode at 1477 (1675) cm^{-1} involve relative motion of the ether oxygen atom with

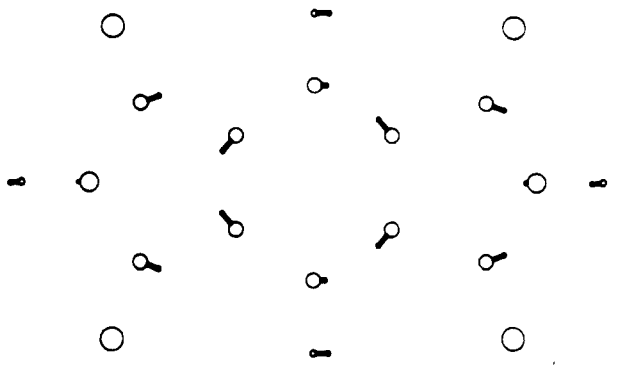

Figure 11. Eigenvector of the B_{3u} mode of PMDA at 1247 (1414) cm^{-1}.

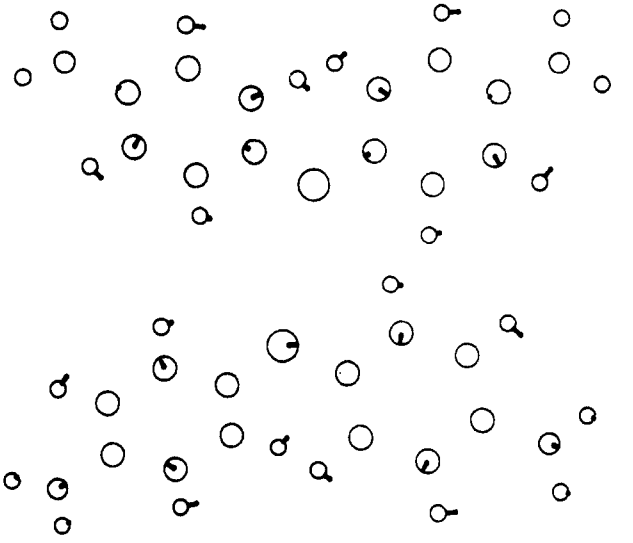

Figure 12. Eigenvector of the B mode of ODA at 1212 (1375) cm^{-1}.

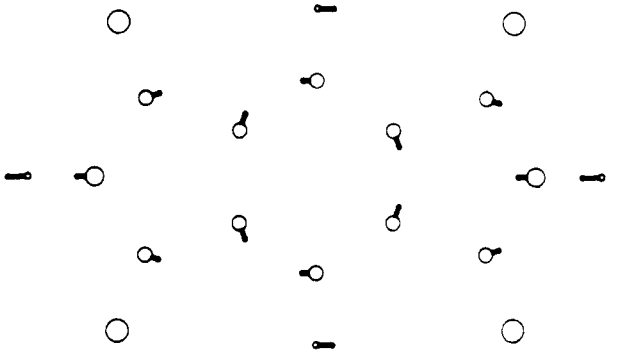

Figure 13. Eigenvector of the B_{3u} mode of PMDA at 1195 (1355) cm^{-1}.

respect to its adjacent covalently coupled carbon atoms. This calculated lower lying ODA mode at 1212 (1375) cm^{-1} might be identified with the observed[14] FT-IR mode at 1252 cm^{-1}. The last of the three modes of our unresolved simulated HREELS triplet is calculated to be at 1195 (1355) cm^{-1}. The eigenvector is shown in Figure 13. This B_{3u} mode of the PMDA molecule is similar to the mode found at 1247 (1414) cm^{-1}. Both involve deformation of the carbon–nitrogen bond. The higher frequency mode, however, involves greater imide ring distortion. This calculated lower lying mode, i.e., the mode at 1195 (1355) cm^{-1}, might be identified with the FT-IR mode observed[14] at 1117 cm^{-1}.

The little peak of Figure 9, slightly above 1000 cm^{-1}, in the valley of the two larger peaks, originates from the

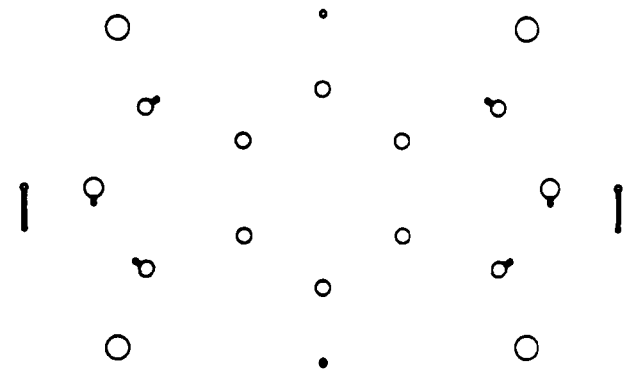

Figure 14. Eigenvector of the B_{2u} mode of PMDA at 1011 (1147) cm^{-1}.

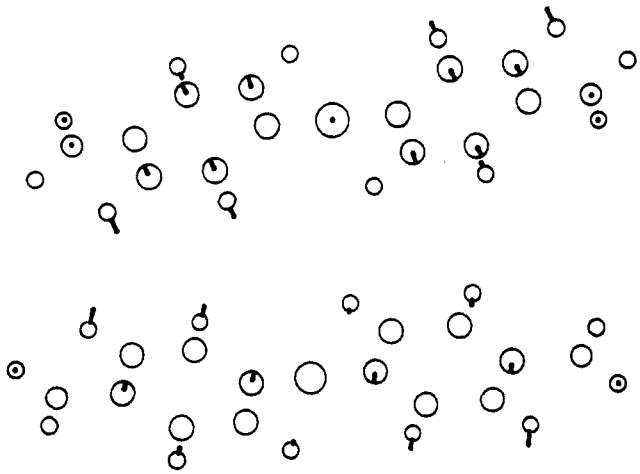

Figure 15. Eigenvector of the A mode of ODA at 876 (994) cm^{-1}.

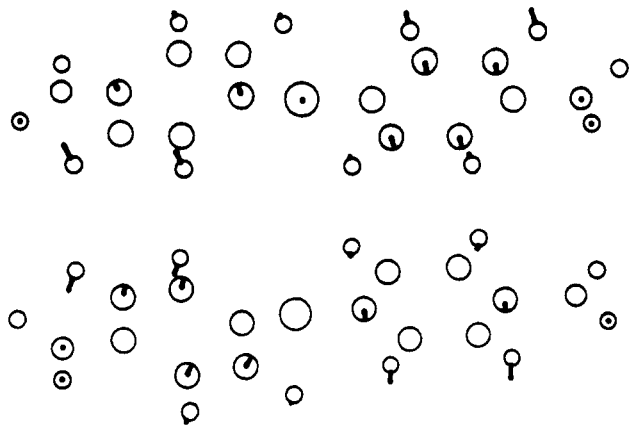

Figure 16. Eigenvector of the B mode of ODA at 873 (990) cm^{-1}.

PMDA B_{2u} mode calculated to be at 1011 (1147) cm^{-1}. The eigenvector is shown in Figure 14. The stronger peak of Figure 9, just below 1000 cm^{-1}, originates from essentially three modes; two ODA modes, one at 876 (994) cm^{-1}, and the other at 873 (990) cm^{-1}; and one PMDA mode calculated to be at 799 (906) cm^{-1}. Views of the eigenvectors of the two ODA modes are given in Figures 15 and 16. The mode at 876 (994) cm^{-1}, of A symmetry, is calculated to contribute approximately less than half of the intensity of the slightly lower frequency ODA mode of B symmetry. The eigenvector of the PMDA B_{1u} mode at 799 (906) cm^{-1} is shown in Figure 17.

One notes that for the PMDA modes, i.e., the one just above 1000 cm^{-1} (Figure 14) and the other just below (Figure 17), there is significant transverse amplitude of the terminal hydrogen atoms. Even though termination of the

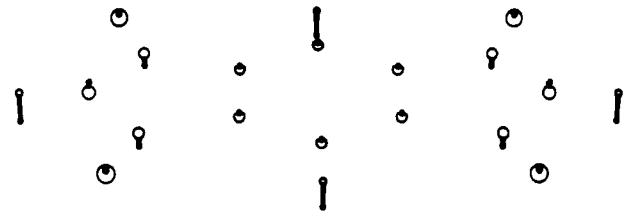

Figure 17. Eigenvector of the B_{1u} mode of PMDA at 799 (906) cm^{-1}.

PMDA fragment by these hydrogen atoms is an artifice to facilitate the calculation, one expects the relatively large transverse amplitude of these "pseudoatoms" to contribute little to the mode frequency since the restoring forces for such transverse motion are small. Most of the contribution to these mode frequencies should come from the relative motions of the other atoms. We should also remark that the PMDA frequency at 799 (906) cm^{-1} has mode displacements that are perpendicular to the plane of the PMDA molecule. To enhance viewing of the eigenvector of this mode in Figure 17, the plane of the molecule has been tilted to obtain a partial edge on view. This is the first PMDA eigenvector with such polarization that we have displayed. All other PMDA modes with such polarization are of lower frequency. Lower frequency modes will clearly be more difficult or perhaps impossible to identify with calculations such as described in this paper. In particular, one might expect collective motion involving both PMDA and ODA units to be responsible for at least some of the observed low-frequency HREELS spectrum. Furthermore, all of the calculated spectra at lower frequency than previously discussed exhibit weak calculated IR intensities.

Finally, it should be stated that the calculations yield many modes over the spectral region examined, for both the PMDA and ODA molecular fragments. Many, however, are infrared inactive. Many are weakly infrared active. Of this entire calculated set of modes, there is only a small number that have been found to have significant calculated infrared intensity. Our previous discussion and identification exhausts all such modes that we have found for both of the molecular units. Furthermore, our identification of FT-IR observed[14] infrared active modes exhausts all of the modes found above 1000 cm^{-1} that have been designated to exhibit medium to strong infrared intensity.

B. Vibrations of the Chromium–PMDA Complex. Mode frequencies and symmetry types obtained from the calculation of the chromium–PMDA complex are also listed in Table IV, along with the values for the uncomplexed PMDA ligand. One sees that the effect of complexing chromium with the PMDA fragment is to reduce all of the carbonyl mode frequencies. The infrared active mode of B_1 symmetry, calculated to be at 1779 (2018) cm^{-1} prior to complexing, has been reduced in frequency by 71 (81) cm^{-1}, whereas the other infrared active mode of B_2 symmetry has been reduced by 43 (49) cm^{-1}. A correspondence can be made between modes obtained before and after complexing the PMDA unit with chromium by correlating the irreducible representations of the higher symmetry point group with the irreducible representations of the lower symmetry point group.[25] For the carbonyl modes, complexing with chromium does not drastically change the eigenvectors of the organic ligand from that obtained prior to complexing. It does, however, change the infrared intensity of the B_{3u} mode.

Figure 18 shows the HREELS-simulated spectrum before and after complexing. We have used the same

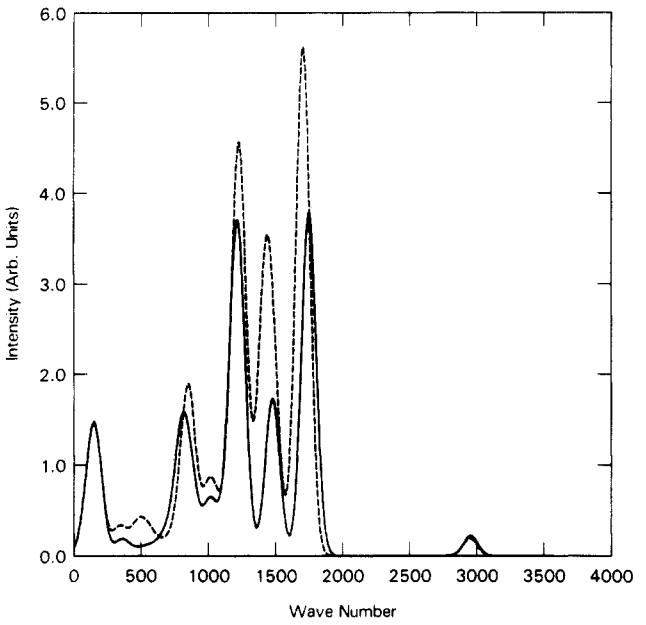

Figure 18. HREELS-simulated spectrum using the HONDO calculated infrared active frequencies. Solid: prior to complexing with chromium (see Figure 9). Dashed: after complexing with chromium.

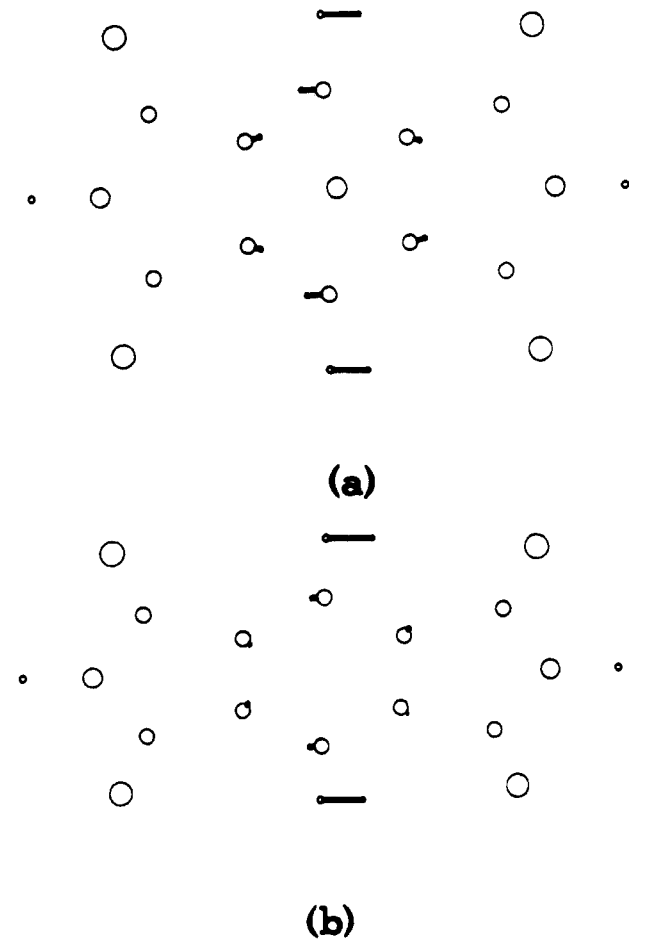

Figure 19. (a) Eigenvector of the B_1 mode at 1415 (1605) cm^{-1} of the Cr–PMDA complex. (b) Eigenvector of the B_{3u} mode of PMDA at 1418 (1608) cm^{-1}, prior to complexing.

Gaussian width, 85 cm^{-1}, in broadening the levels to generate both curves. One sees the downshifted carbonyl frequency of the complex with, however, considerably enhanced intensity. This can be traced to the intensity increase of the B_1 mode with polarization along the long axis of the molecule. The increase in intensity for this mode is a result of significant enhancement of the induced dipole moment along the long axis of the molecule for displacements of the carbonyl carbon and oxygen atoms along the short axis of the molecule.

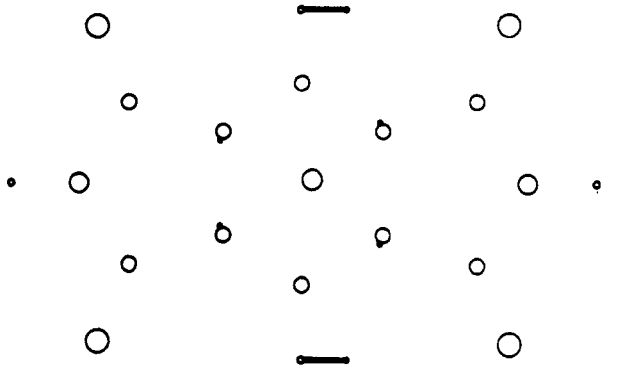

Figure 20. Eigenvector of the B_1 mode at 1242 (1409) cm^{-1} of the Cr–PMDA complex.

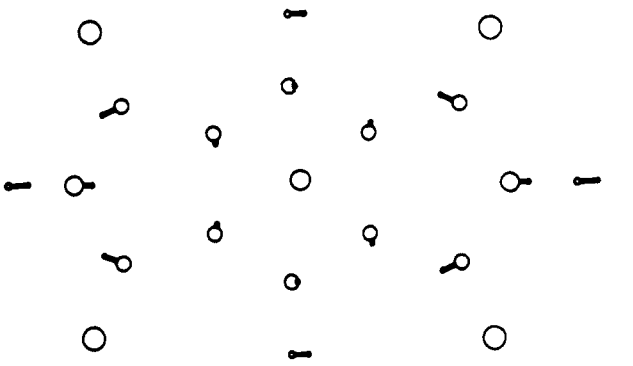

Figure 21. Eigenvector of the B_1 mode at 1226 (1391) cm^{-1} of the Cr–PMDA complex.

In the vicinity, but just below the ODA mode at 1477 (1675) cm^{-1} of the clean material, we see a strong increase in intensity. This arises from a PMDA infrared active mode of B_1 symmetry at 1415 (1605) cm^{-1}. The eigenvector of this mode is shown in Figure 19a. It is of interest that a mode of the clean material near this frequency and with correlated symmetry type B_{3u} exhibits little infrared strength. The eigenvector of this weak infrared active mode at 1418 (1608) cm^{-1} is shown in Figure 19b. We have not listed the frequency of this mode in Table IV to emphasize that the calculated intensity suggests that it is unobservable. Note that both of these symmetry-correlated modes involve in-phase motion of four carbon atoms on the central PMDA benzene ring. The relative amplitude of these carbon atoms for the chromium complex (Figure 19a) is, however, significantly enhanced over their displacement in the clean material (Figure 19b). One should also recall that these carbon sites are the sites of enhanced LUMO amplitude prior to complexing. Consequently, these four carbon atoms accept most of the electronic charge from the chromium atom (see Table III). One therefore expects the large dipole moment and hence strong infrared intensity to arise from the enhanced electronic charge at these carbon atom sites as well as from the enhanced displacements of these atoms. At lower frequency, near 1200 cm^{-1}, we had a peak composed of essentially three infrared active modes prior to complexing. Two of the contributions were from the PMDA unit. Upon complexing, these two PMDA modes of B_1 symmetry are now found at 1242 (1409) and 1226 (1391) cm^{-1}. The corresponding eigenvectors are given in Figures 20 and 21. Since the ODA contribution remains unchanged and one

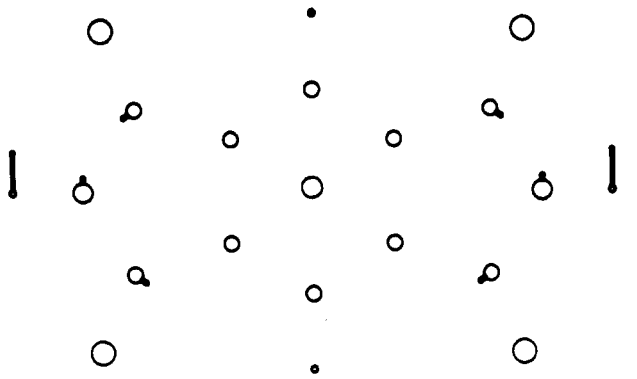

Figure 22. Eigenvector of the B_2 mode at 1017 (1154) cm^{-1} of the Cr–PMDA complex.

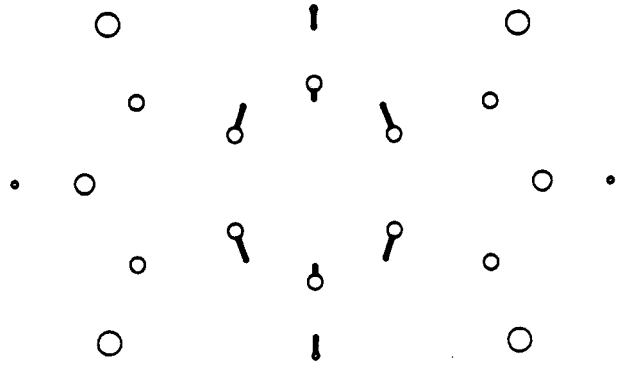

Figure 23. Eigenvector of the A_g mode of PMDA at 1558 (1767) cm^{-1}.

PMDA contribution is essentially unshifted, whereas the other is shifted up in frequency by 32 (36) cm^{-1}, the calculated HREELS feature is found at essentially the same frequency. There is an increase in calculated intensity, presumably related to the additional electronic charge on the atoms of the ligand after complexing.

The little peak that we had found at 1011 (1147) cm^{-1}, of the clean material, remains relatively unchanged. It moves upon complexing to 1017 (1154) cm^{-1}, with the eigenvector given in Figure 22.

The HREELS-calculated peak just below 1000 cm^{-1} was composed of PMDA and ODA components. The PMDA B_{1u} mode previously found at 799 (906) cm^{-1} is now found at 840 (953) cm^{-1}, with somewhat greater intensity and of symmetry type A.

Overall, one notes generally that our simulated HREELS spectrum exhibits greater intensity for the complex than for the clean material. This is presumably due the the increase in electronic charge at the atomic centers of the PMDA fragment as a result of charge transfer from the chromium atom.

Finally, we discuss one last mode of interest, namely, the infrared inactive PMDA breathing mode of A_g symmetry for the clean material, found at 1558 (1767) cm^{-1}, with the eigenvector shown in Figure 23. Examination of the relative displacements of the carbon atoms on the central benzene ring suggests that this mode should perhaps exhibit the largest change in frequency upon formation of the chromium half-sandwich complex. This is indeed found, for upon complexing, this mode, now of A_1 symmetry, is calculated to be at 1383 (1569) cm^{-1}, i.e., downshifted by 175 (198) cm^{-1}.

All modes of the chromium–PMDA complex that we have illustrated have negligible atomic displacements normal to the least-squares plane through the buckled aromatic ligand. Therefore, only the view along the normal to this plane has been shown.

V. Discussion and Conclusions

The present study was motivated for essentially two reasons. First, we wanted to view the normal mode displacements of the PMDA–ODA polyimide. Second, we wanted to see what sort of changes could be expected upon deposition of a metal, e.g., chromium, during the incipient stages of interface formation.

Detailed comparison with the results of HREELS experiments involving metal atom deposition will be difficult, and it is important to issue a number of disclaimers. First, we have examined a complex involving one single metal atom and ligand. One expects that at all but the lowest deposition regimes one will have significant metal atom clustering. At the lowest deposition regimes, one might expect a significant number of single metal atom interaction sites provided the conditions preclude significant metal atom diffusion. Furthermore, spectral changes induced by metal atom deposition at the lowest depositions are difficult to observe due to decreased sensitivity. Also, even though one has truly achieved incipient formation of the metal–polymer interface, interpretation of the data will not be straightforward for the following two reasons. First; at low deposition, there will be a mixture of reacted and unreacted material. This will broaden and wash out sharp spectral features. It will, therefore, be necessary to perform an average over calculated spectra derived from reacted and unreacted species in an attempt to reproduce or simulate the experimental spectrum. Second; even though one is in a predominantly single metal atom interaction regime, one expects more than one single type of interaction site to be present. Different single atom interaction sites, while exhibiting qualitative similar behavior, will exhibit induced spectral changes that are numerically different and lead to a further washing out of the spectrum. The half-sandwich structure that we have treated is an abstraction in the sense that the chromium metal atom will attempt to achieve a greater degree of coordination dependent upon the local geometry that it experiences. We have examined a number of differently coordinated single metal atom complexes with the result that even though the results obtained are qualitatively similar, arising from back-charge donation from the chromium atom to the ligand, the actual calculated changes upon complexing are numerically different. Finally, no detailed comparison between the results of calculation and the observed HREELS spectrum will be on firm ground until the electron-scattering selection rules are more thoroughly understood.

With the previous qualifications in mind, examination of the chromium–PMDA complex was, therefore, predominantly motivated for an essentially heuristic reason. We wanted to see what sort of changes in the HREELS spectrum might be generally expected upon the initial interaction between the metal atom and the PMDA–ODA polymer. The calculated induced spectral changes that we have found can be summarized as follows:

1. Softening of the carbonyl vibrations. Along with these frequency shifts, one can expect changes in HREELS intensity, reflecting essentially changes in IR intensities.
2. Appearance of a new spectral feature. We have shown how an infrared mode of low intensity can exhibit significantly increased intensity upon complexing so that it yields a prominent feature in the simulated HREELS spectrum.
3. Significant changes in infrared inactive modes. The greatest frequency shift was found for an infrared inactive breathing mode. For a chromium–PMDA complex dis-

tributed throughout the bulk of the polymer film, such a mode might be observed in the Raman spectrum. At or near the PMDA–ODA surface, it might be observed in the HREELS impact scattering regime.

A previous HREELS study[4] of chromium deposition onto the PMDA–ODA surface has revealed the disappearance of the carbonyl peak with the appearance of an HREELS feature approximately 200 cm^{-1} below. It would be of interest to perform similar measurements at coverages significantly less than the chromium monolayer coverage reported.

Another feature of interest found upon complexing PMDA with a chromium atom is the overall enhancement of the FT-IR/HREELS intensities. This may not be straightforward to observe since it is generally not a simple matter to calibrate absolute experimental intensities. At any but the lowest concentrations of chromium, one expects the overall magnitude of the intensity to be attenuated upon successive chromium depositions. Perhaps such intensity enhancement as found in the present calculations can be observed at the lowest concentration regimes.

Acknowledgment. I am indebted to A. R. Rossi for making the HONDO 7 molecular orbital program available to me and for assistance with its execution.

Registry No. (PMDA)(ODA) (copolymer), 25038-81-7; (PMDA)(ODA) (SRU), 25036-53-7.

References and Notes

(1) DiNardo, N. J.; Demuth, J. E.; Clarke, T. C. *J. Chem. Phys.* **1986**, *85*, 6739.
(2) Pireaux, J. J.; Gregoire, C.; Thiry, P. A.; Caudano, R. *J. Vac. Sci. Technol.* **1987**, *A5*, 598.
(3) DiNardo, N. J.; Demuth, J. E.; Clarke, T. C. *J. Vac. Sci. Technol.* **1986**, *A4*, 1050.
(4) DiNardo, N. J.; Demuth, J. E.; Clarke, T. C. *Chem. Phys. Lett.* **1985**, *121*, 239.
(5) Pireaux, J. J.; Vermeersch, M.; Gregoire, C.; Thiry, P. A.; Caudano, R. *J. Chem. Phys.* **1988**, *88*, 3353.
(6) Hahn, P. O.; Rubloff, G. W.; Ho, P. S. *J. Vac. Sci. Technol.* **1984**, *A2*, 756.
(7) White, R. C.; Haight, R.; Silverman, B. D.; Ho, P. S. *Appl. Phys. Lett.* **1987**, *51*, 481.
(8) Ho, P. S.; Hahn, P. O.; Bartha, J. W.; Rubloff, G. W.; Legoues, F. K.; Silverman, B. D. *J. Vac. Sci. Technol.* **1985**, *A3*, 739.
(9) Atanasoska, L. J.; Anderson, S. G.; Meyer, H. M., III; Lin, Z.; Weaver, J. H. *J. Vac. Sci. Technol.* **1987**, *A5*, 3325.
(10) Silverman, B. D.; Sanda, P. N.; Ho, P. S.; Rossi, A. R. *J. Polym. Sci., Polym. Chem. Ed.* **1985**, *23*, 2857.
(11) Silverman, B. D.; Bartha, J. W.; Clabes, J. G.; Ho, P. S.; Rossi, A. R. *J. Polym. Sci., Polym. Chem. Ed.* **1986**, *24*, 3325.
(12) Silverman, B. D.; Sanda, P. N.; Clabes, J. G.; Ho, P. S.; Hofer, D. C.; Rossi, A. R. *J. Polym. Sci., Polym. Chem. Ed.* **1988**, *26*, 1199.
(13) Rossi, A. R.; Sanda, P. N.; Silverman, B. D.; Ho, P. S. *Organometallics* **1987**, *6*, 580.
(14) Ishida, H.; Wellinghoff, S. T.; Baer, E.; Koenig, J. L. *Macromolecules* **1980**, *13*, 826.
(15) Dupuis, M.; Watts, J. D.; Villar, H. O.; Hurst, G. J. B. HONDO Version 7, IBM Corporation, Scientific and Engineering Computations, Kingston, NY, 12401.
(16) Binkley, J. S.; Pople, J. A.; Hehre, W. J. *J. Am. Chem. Soc.* **1980**, *102*, 939.
(17) Takahashi, N.; Yoon, D. Y.; Parrish, W. *Macromolecules* **1984**, *17*, 2583.
(18) Dobbs, K. D.; Hehre, W. J. *J. Comp. Chem.* **1987**, *8*, 861.
(19) Graphics software from the Scientific and Engineering Computations Group, IBM Data Systems Division, Kingston, NY.
(20) Villar, H. O.; Dupuis, M.; Watts, J. D.; Hurst, G. J. B.; Clementi, E. *J. Chem. Phys.* **1988**, *88*, 1003.
(21) Amos, R. D.; Gaw, J. F.; Handy, N. C.; Carter, S. *J. Chem. Soc., Faraday Trans. 1* **1988**, *84*, 1247.
(22) Ibach, H.; Mills, D. L. *Electron Energy Loss Spectroscopy and Surface Vibrations*; Academic Press: New York, 1982.
(23) Thiry, P. A.; Liehr, M.; Pireaux, J. J.; Caudano, R. *Phys. Scr.* **1987**, *35*, 368.
(24) Johnson, C. K. ORTEP-II; A Fortran Thermal-Ellipsoid Plot Program For Crystal Structure Illustrations. Report ORNL-5138, 1976; Oak Ridge National Laboratory, Oak Ridge, TN.
(25) Burns, G. *Introduction to Group Theory with Applications*; Academic Press: New York, 1977; Appendix 7.

Crystal Structure of Poly(4-methyl-*m*-phenylene terephthalamide)

Kenji Okuyama,* Hiroyuki Hidaka, and Hironobu Ichige

Faculty of Technology, Tokyo University of Agriculture and Technology, Koganei, Tokyo 184, Japan

Masanori Osawa

Central Research Laboratory, Mitsui-Toatsu Chemicals, Inc., Kasama-cho, Totsuka-ku, Yokohama-shi, Kanagawa 247, Japan. *Received January 17, 1989; Revised Manuscript Received February 23, 1989*

ABSTRACT: The conformation and molecular packing of poly(4-methyl-*m*-phenylene terephthalamide) has been determined by X-ray diffraction. Unit cell dimensions were a = 8.57, b = 7.54, c (fiber axis) = 22.11 Å, $\alpha = \gamma = 90°$, and $\beta = 116.3°$. The space group symmetry was *I*1*a*1. A model with parallel 1/1 helices at the corner and center of the unit cell was refined simultaneously against X-ray intensity data and stereochemical restraints. Mainly because of the methyl moiety substituted to the *m*-phenylene, the torsion angles of the benzene rings measured from the amide planes were fairly deviated from the energetically stable angle. The polymer chains form a two-dimensional hydrogen-bonded network with bond lengths of about 2.8 Å, which makes the crystal structure very stable. The molecular cross-section and the packing coefficient of this polymer showed that the polymer chains were packed rather loosely compared with other wholly aromatic polyamides.

Introduction

Fibers made of poly(*p*-phenylene terephthalamide) and its isomer, poly(*m*-phenylene isophthalamide) (hereafter, abbreviated PPTA and MPIA, respectively), have been utilized in many fields because of their high thermal stability (decomposition temperature T_d = 500 and 415 °C, respectively). Poly(4-methyl-*m*-phenylene terephthalamide) (4M-MPTA), is a stereochemically intermediate compound of the above two aromatic polyamides with methyl substituent. In addition to the high thermal stability (T_d = 425 °C), 4M-MPTA shows good dimensional stability at high temperature, good morphological stability against flame, and good dyeing ability.[1] For example, fibers of 4M-MPTA shrink only by 18% of their original length at 480 °C. On the other hand, those of MPIA shrink by 61% and fuse together at the same temperature.

0024-9297/89/2222-3776$01.50/0